JOURNAL OF BACTERIOLOGY, May 2008, p. 3632–3645 Vol. 190, No. 10
0021-9193/08/$08.00+0 doi:10.1128/JB.01999-07

Enterococcus faecalis PcfC, a Spatially Localized Substrate Receptor for Type IV Secretion of the pCF10 Transfer Intermediate▽

Yuqing Chen,[1] Xiaolin Zhang,[1] Dawn Manias,[2] Hye-Jeong Yeo,[3] Gary M. Dunny,[2] and Peter J. Christie[1]*

Department of Microbiology and Molecular Genetics, University of Texas Medical School at Houston, 6431 Fannin, Houston, Texas 77030[1]; Department of Microbiology, University of Minnesota Medical School, 1460 Mayo Bldg., MMC 196, 420 Delaware St., S.E., Minneapolis, Minnesota 55445[2]; and Department of Biology and Biochemistry, University of Houston, Houston, Texas 77204[3]

Received 21 December 2007/Accepted 25 February 2008

Upon sensing of peptide pheromone, *Enterococcus faecalis* efficiently transfers plasmid pCF10 through a type IV secretion (T4S) system to recipient cells. The PcfF accessory factor and PcfG relaxase initiate transfer by catalyzing strand-specific nicking at the pCF10 origin of transfer sequence (*oriT*). Here, we present evidence that PcfF and PcfG spatially coordinate docking of the pCF10 transfer intermediate with PcfC, a membrane-bound putative ATPase related to the coupling proteins of gram-negative T4S machines. PcfC and PcfG fractionated with the membrane and PcfF with the cytoplasm, yet all three proteins formed several punctate foci at the peripheries of pheromone-induced cells as monitored by immunofluorescence microscopy. A PcfC Walker A nucleoside triphosphate (NTP) binding site mutant (K156T) fractionated with the *E. faecalis* membrane and also formed foci, whereas PcfC deleted of its N-terminal putative transmembrane domain (PcfCΔN103) distributed uniformly throughout the cytoplasm. Native PcfC and mutant proteins PcfCK156T and PcfCΔN103 bound pCF10 but not *pcfG* or Δ*oriT* mutant plasmids as shown by transfer DNA immunoprecipitation, indicating that PcfC binds only the processed form of pCF10 in vivo. Finally, purified PcfCΔN103 bound DNA substrates and interacted with purified PcfF and PcfG in vitro. Our findings support a model in which (i) PcfF recruits PcfG to *oriT* to catalyze T-strand nicking, (ii) PcfF and PcfG spatially position the relaxosome at the cell membrane to stimulate substrate docking with PcfC, and (iii) PcfC initiates substrate transfer through the pCF10 T4S channel by an NTP-dependent mechanism.

The type IV secretion (T4S) systems are ancestrally related to bacterial conjugation machines and are used by many species of gram-negative and gram-positive bacteria as well as the thermophilic archaeon *Sulfolobus* (19, 31, 32, 61). Most T4S systems translocate DNA or protein substrates directly to target cells by a cell contact-dependent process, and some alternatively translocate substrates to or from the milieu (5, 6, 20). Many systems translocate DNA substrates within or between bacterial species, although a large number of systems have been adapted by pathogenic species to deliver DNA or protein substrates to fungal, plant, or human cells (7, 17, 53). The T4S systems are composed of an envelope-spanning secretion channel and a surface structure such as a pilus for gram-negative bacteria or a protein adhesin for gram-positive bacteria to mediate attachment to target cells (1, 20, 32). These general properties—a wide phylogenetic distribution, functional versatility, and structural diversity—make T4S systems excellent subjects for mechanistic studies exploring the evolution of biological complexity. At this time, however, detailed structure-function comparisons are not possible due to the paucity of information available for systems other than a few gram-negative models, e.g., the conjugation systems encoded by F, RP4, and R388 plasmids and the *A. tumefaciens* VirB/D4 T4S system.

Here, we initiated studies of the pheromone-inducible conjugation system of the *Enterococcus faecalis* plasmid pCF10 (25). This 67.6-kb plasmid is a member of the family of sex pheromone plasmids found to date only in the enterococci but with the capacity to mobilize transfer of *oriT*-containing plasmids to *Lactococcus lactis* and *Streptococcus agalactiae* (64). pCF10 carries the tetracycline resistance conjugative transposon Tn*925* (22) and codes for pheromone sensing and response functions, conjugation functions, and a surface adhesin termed aggregation substance (AS) which is important both for conjugation and virulence (38, 68, 69). In addition to its medical importance as a reservoir for antibiotic resistance and other virulence traits, the pCF10 transfer system is an attractive model gram-positive T4S system for mechanistic analysis because T4S machine assembly and function are tightly controlled at the transcriptional level, many features of pheromone-inducible regulation are known, and very high plasmid transfer rates are achieved soon after induction (25, 38).

Bacterial conjugation can be viewed as three biochemical reactions coupled in time and probably also in space. One or more processing factors termed the DNA transfer and replication (Dtr) proteins initiate transfer by assembling as a relaxosome at the origin of transfer sequence (*oriT*) to catalyze cleavage of the DNA strand (T strand) destined for transfer (33). For pCF10, the PcfG relaxase and the accessory factor PcfF function together to cleave DNA at the *nic* site within an IncP-type *oriT* sequence (18, 64). Next, by a mechanism that is poorly understood, the relaxosome or the processed transfer intermediate interacts with a substrate receptor, also termed

* Corresponding author. Mailing address: Department of Microbiology and Molecular Genetics, University of Texas Medical School at Houston, 6431 Fannin, Houston, TX 77030. Phone: (713) 500-5440. Fax: (713) 500-5499. E-mail: Peter.J.Christie@uth.tmc.edu.

▽ Published ahead of print on 7 March 2008.

the type IV coupling protein (T4CP) (3). These membrane proteins are components of all conjugation systems characterized to date and are related in sequence and overall structure to the ATP-dependent DNA translocases FtsK and SpoIIIE (27, 30). For pCF10, the putative T4CP is PcfC, whose sequence features include an N-terminal putative transmembrane (TM) domain, conserved Walker A and B nucleoside triphosphate (NTP) binding motifs, and other motifs common to this protein family (60; this study). In a final reaction, the T4CP delivers the DNA substrate to a cognate T4S transport apparatus for substrate transfer across the bacterial cell envelope (16, 19, 61). The mating pair formation (Mpf) proteins are responsible for target cell attachment and formation of tight mating junctions and a membrane-spanning channel between donor and recipient cells. In the case of pCF10, a ~15-kb region situated between *prgB* (codes for AS) and *pcfC* is predicted encode the translocation channel (18).

The DNA processing reactions of several gram-positive conjugative plasmids have been characterized in detail (14, 15, 18, 46, 63, 64). By contrast, structure-function studies of the cognate mating pair formation and substrate transfer mechanisms are still in their infancy, although an interaction network for putative Mpf subunits of the *S. agalactiae* pIP501-encoded T4S system recently was described (1). In this study, we have examined the question of how pCF10 substrate processing is coupled to translocation at the cell membrane. Our cytological and biochemical findings indicate that the PcfF and PcfG processing factors not only catalyze the *oriT* nicking reaction but also spatially position the relaxosome at several sites on the membrane, most probably in proximity to the PcfC substrate receptor. PcfF and PcfG deliver the processed form of pCF10 to PcfC, a substrate receptor for the pCF10 transfer system, and in turn PcfC energizes substrate transfer through the pCF10-encoded mating channel.

MATERIALS AND METHODS

Bacterial strains and growth conditions. Bacterial strains, plasmids, and oligonucleotides are listed in Table 1. *Escherichia coli* DH5α (Gibco-BRL) and EC1000, a strain that produces the pWV01 RepA protein (48), were used as hosts for plasmid constructions. *E. coli* BL21(DE3) (Novagen) was used for protein production. *E. coli* strains were cultured in Luria broth (LB) or brain heart infusion broth (BHI) (Difco Laboratories) and grown at 37°C with shaking. *E. faecalis* strains were cultured in BHI and grown at 37°C without shaking. Antibiotics were added at the following final concentrations: for *E. faecalis*, erythromycin at 100 μg ml^{-1} for plasmid markers and 10 μg ml^{-1} for chromosomal markers, fusidic acid at 25 μg ml^{-1} rifampin at 200 μg ml^{-1}, chloramphenicol at 10 μg ml^{-1}, spectinomycin at 1,000 μg ml^{-1} for plasmid markers and 250 μg ml^{-1} for chromosomal markers, streptomycin at 1,000 μg ml^{-1}, at tetracycline at 10 μg ml^{-1}; for *E. coli*, carbenicillin at 50 μg ml^{-1}, chloramphenicol at 20 μg ml^{-1}, erythromycin at 100 μg ml^{-1}, kanamycin at 50 μg ml^{-1}, and spectinomycin at 50 μg ml^{-1}. All antibiotics were obtained from Sigma Chemical Co.

Plasmid constructions. Plasmid pCY32 was constructed as follows to delete *pcfC* from pCF10. An 825-bp region immediately 5′ of *pcfC* (upstream fragment) was amplified with the primer pair pcfC-1/pcfC-2. A 945-bp region immediately 3′ of *pcfC* (downstream fragment) was amplified with the primer pair pcfC-3/pcfC-4. The two fragments were cloned sequentially into pCJK47 (Table 1) to create pCY32 with the primer-added NcoI/SmaI (upstream fragment) and SmaI/XbaI (downstream fragment) restriction sites. pCY32 was used to delete *pcfC* from pCF10 by marker exchange as described previously (42).

Plasmid pCY24 expressing *pcfC* from the nisin-inducible promoter P_{nis} was constructed by PCR amplification of *pcfC* with the primer pair BspHI-pcfC and pcfC-R-XhoI (Table 1), digestion of the PCR product with BspHI and XhoI, and introduction into NcoI/XhoI-digested pMSP3545 (Table 1). Plasmid pCY25 expressing *pcfC* from the constitutive promoter P_{23} from *Lactococcus lactis* was constructed as follows. Plasmid pCIp23 carries promoter P_{23} from pDL278p23, introduced as a 0.2-kb EcoRI/BamHI restriction fragment into similarly digested pCI372. Plasmid pCY25, expressing the *pcfC* gene from promoter P_{23}, was constructed by PCR amplification of *pcfC* from pCF10 with primer pairs BsaI-B-pcfC and pcfC-PstI, digestion of the PCR product with BsaI and PstI, and introduction of the resulting fragment into BamHI/PstI-digested pCIp23. Plasmid pCY31 expressing *pcfCΔN103* (lacks codons 1 to 103) from promoter P_{23} was constructed by PCR amplification of *pcfCΔN103* with primer pair RBS-C (a sequence containing an optimal ribosomal binding site was added to the primer) and ΔN103R and introduction of the PCR fragment into pGEM-T Easy. The *pcfCΔN103* allele, recovered as an SphI fragment, was introduced into similarly digested pDL278p23. The orientation of *pcfCΔN103* relative to P_{23} was verified by restriction enzyme analysis.

Plasmid pCY26 expressing *GST-pcfCΔN103* was constructed by amplification of *pcfC′* starting at codon 103 with primers GST-PcfC-Δ103-F/GST-PcfC-R, digestion with BamHI and EcoRI, and introduction into similarly digested pGEX2T. Plasmid pCY27 expressing *his$_6$-pcfCΔN103* was constructed by amplification of *pcfC′* starting at codon 103 with primers pcfCΔN103-F and pcfC-R-XhoI, digestion with NdeI and XhoI, and introduction into similarly digested pAP1. PcfC derivatives with Walker A mutations were constructed as follows. The invariant Lys156 within the Walker A motif of PcfC was mutated by QuikChange (Stratagene) site-directed mutagenesis according the manufacturer's instructions. Plasmids pCY25, pCY26, and pCY27 served as templates for PCR amplification with the *Pfu Turbo* polymerase using complementary oligonucleotides pcfC-K/T-5 and pcfC-K/T-3 to construct a Lys156Thr (K156T) substitution. Plasmids pCY28, pCY29, and pCY30 were sequenced across the entire *pcfC* gene to confirm introduction of the K156T mutation and lack of undesired mutations.

Plasmid pCY34 expressing P_{tac}-*GST-pcfF* was constructed by PCR amplification of *pcfF* with primer pair GSTF5 (BamHI and NdeI sites added to the primer) and GSTF3 (XhoI site added to the primer), and the BamHI-XhoI-digested product was cloned into similarly digested pGEX6p-1.

Conjugation assays. *E. faecalis* donor and recipient cultures grown overnight were diluted 1:10 in fresh BHI and incubated at 37°C for 1 h. Donor and recipient cells were mixed at a ratio of 1:10 and mated for 1 h at 37°C. Serial dilutions of the mating mixtures were plated on selective BHI agar plates to obtain CFU of transconjugants and donors. Plasmid transfer was expressed as transconjugants per donor, and experiments were carried out in triplicate (18).

Cell fractionation and protein detection. Exponential-phase cultures (10 ml) of *E. faecalis* strains carrying pCF10 or various pCF10 mutants were induced with 20 ng/ml of peptide cCF10 for 1.5 h. Exponential-phase *E. faecalis* strains were incubated with 20 ng/ml of nisin (Sigma) for 2 h to induce expression from the nisin-inducible promoter P_{nis} (37). Equivalent numbers of cells were pelleted by centrifugation at 5,000 × *g* for 10 min at 4°C and washed once with cold 1× physiologically buffered saline (PBS). Cells were frozen at −20°C overnight, thawed, and treated with 200 μl of lysozyme solution (10 mM Tris-HCl [pH 8.0], 50 mM NaCl, 1 mM EDTA, 20% sucrose, 15 mg/ml lysozyme, 10 μg/ml mutanolysin) at 37°C for 20 min. The protoplasts were resuspended in 1 ml of lysis buffer (20 mM Tris-HCl [pH 8.0], 150 mM NaCl, 1 mM EDTA, 1× protease inhibitor cocktail [Roche]) and lysed with sonication (Branson 250 microtip sonicator). Unlysed cells were removed by centrifugation twice at 15,700 × *g* for 30 min. The soluble lysates were subjected to ultracentrifugation at 165,000 × *g* for 2 h at 4°C. The supernatant contained the cytoplasmic fraction. The pellet was resuspended by sonication in 1 ml of lysis buffer and was again subjected to ultracentrifugation to remove residual cytoplasmic proteins. The pellet was resuspended in 1 ml of lysis buffer containing 1% Triton X-100. Cytoplasmic and membrane fractions were applied on a per-cell equivalent basis onto sodium dodecyl sulfate (SDS)-polyacrylamide gels and proteins of interest identified by Western transfer and immunostaining, as previously described (9).

To monitor PcfC, -F, and -G protein production over time following pheromone induction, equivalent numbers of cells were harvested at the indicated time points. After treatment with lysozyme solution (10 mM Tris-HCl [pH 8.0], 50 mM NaCl, 1 mM EDTA, 20% sucrose, 15 mg/ml lysozyme) at 37°C for 15 min, protoplasts were lysed by boiling for 5 min in the lysis buffer (20 mM Tris-HCl [pH 8.0], 150 mM NaCl, 1 mM EDTA, 1% Triton X-100) and analyzed by SDS-polyacrylamide gel electrophoresis (SDS-PAGE) and Western blot analysis.

Protein purification. The proteins His_6-PcfCΔN103, His_6-PcfCΔN103K156T, His_6-PcfF, and PcfG-His_6 were produced in strain BL21(DE3) carrying pCY27, pCY30, pCY33, and pCY36, respectively. Bacteria were grown at 37°C in 100 ml of LB medium supplemented with 50 μg/ml kanamycin until the culture reached an absorbance at 600 nm of ~0.4. Isopropyl-β-D-thiogalactoside (Anatrace) was added to a final concentration of 0.1 mM, cells were incubated at 30°C for 3 h, and bacteria were pelleted by centrifugation at 6,000 × *g* for 20 min. Cell pellets

TABLE 1. Bacterial strains, plasmids, and oligonucleotides used in this study

Strain, plasmid, or oligonucleotide	Relevant features or sequence (5′→3′)	Source or reference
Strains		
E. coli		
DH5α	F$^-$ ϕ80d*lacZ* ΔM15 Δ(*lacZYA-argF*)*U169 deoR recA1 endA1 hsdR17*(r_K^- m_K^+) *phoA supE44* λ$^-$ *thi-1 gyrA96 relA1*	Gibco-BRL
BL21 (DE3)	F$^-$ *ompT* r_B^- m_B^- DE3	Novagen
EC1000	*E. coli* cloning host, provides RepA in *trans*	48
E. faecalis		
CK104	OG1RFΔ*upp2*	43
OG1ES	Erm^r Str^r	64
OG1SSp	Str^r Spc^r	26
Plasmids		
Expression plasmids/vectors		
pET-28a, b(+)	Kan^r, expression vector for His tagging	Novagen
pAP1	Kan^r, pET-28a(+) derivative	12
pGEX2T	Crb^r, expression vector for GST tagging	Amersham
pGEX6P-1	Crb^r, expression vector for GST tagging	Amersham
pGEM-T Easy	Crb^r, TA cloning vector	Promega
pCI372	Cam^r, shuttle vector	35
pDL278	Spc^r, shuttle vector	70
pDL278p23	Spc^r, pDL278 with *L. lactis* constitutive promoter P_{23}	18
pCIp23	Cam^r, pCI372 with promoter P_{23}	This study
pCJK47	Carries $oriT_{pCF10}$, *lacZ*, and P-*phe*S* cassette	42
pMSP3535	Erm^r, shuttle vector, inducible promoter P_{nis}	10
pMSP3545	Erm^r, shuttle vector, inducible promoter P_{nis}	10
pCJK21	Erm^r Spc^r, shuttle vector, inducible promoter P_{nis}	43
pCF10 derivatives		
pCF10	Pheromone-inducible conjugative plasmid	24
pCF10Δ*pcfC*	pCF10 deleted of *pcfC*	This study
pCF10Δ*pcfF*	pCF10 deleted of *pcfF*	18
pCF10*pcfG*	pCF10 with *pcfG* inactivated by Ll.ltrBΔORF-Kan insertion	64
pCF10Δ*oriT*	pCF10 deleted of *oriT*	64
pcfC expression plasmids		
pCY24	pMSP3545 expressing P_{nis}-*pcfC*	This study
pCY25	pCIp23 expressing P_{23}-*pcfC*	This study
pCY26	pGEX2T expressing P_{tac}-*GST-pcfCΔN103*	This study
pCY27	pAP1 expressing P_{T7}-*his6-pcfCΔN103*	This study
pCY28	pCIp23 expressing P_{23}-*pcfCK156T*	This study
pCY29	pGEX2T expressing P_{tac}-*GST-pcfCΔN103;K156T*	This study
pCY30	pAP1 expressing P_{T7}-*his6-pcfCΔN103;K156T*	This study
pCY31	pDL278p23 expressing P_{23}-*pcfCΔN103*	This study
pCY32	pCJK47 with *pcfC* flanking sequences for construction of pCF10Δ*pcfC*	This study
pcfF expression plasmids		
pCY33	pET-28b(+) expressing *his$_6$-pcfF*	18
pCY34	pGEX6p-1 expressing *GST-pcfF*	This study
pCY16	pDL278p23 expressing P_{23}-*pcfF*	18
pcfG expression plasmids		
pCY36	pET-28 b(+) expressing *pcfG-his$_6$*	18
pCY19	pCJK21 expressing P_{nis}-*pcfG*	18
Oligonucleotides		
pcfC-PstI	AACTGCAGTTAAACGTGTGTTTCTTCTTTC	
BsaI-B-pcfC	CATGGTCTCGGATCCACGTGGGTAAAATTGATCAAAC	
pcfC-K/T-5	ATCGCCATTCTAGGTGATTCTGGAGCGGCCACCACGTTAGCTTTT	
pcfC-K/T-3	GGCCGCTCCAGAATCACCTAGAATGGCGATATTCTTATTTTTTTG	
GST-pcfC-Δ103-F	CATGGTCTCGGATCCGCTCGTTTTGCTACACCTGC	
GST-pcfC-R	CATGGTCTCGAATTCTTAAACGTGTGTTTCTTCT	
pcfCΔN103-F	GCTCGTTTTCATATGGCTACACCTGC	
pcfC-R-XhoI	AACGCACGTCCTCGAGCTATTAGGCTAGAACGTGTGTTTC	
pcfC-1	ATGGTACCGAGCAACCAGATGAAATAGC	

Continued on following page

TABLE 1—*Continued*

Strain, plasmid, or oligonucleotide	Relevant features or sequence (5′→3′)	Source or reference
pcfC-2	CGCCCGGGACAGTTTCCTTCCTTT	
pcfC-3	CGCCCGGGAAAGACGTGCGTT	
pcfC-4	CGTCATTATCTAGAGCCAAAACAAGTTGG	
TriP-ChromF	TTACCAGTTTTGCAGTAGGG	
TriP-ChromR	TTCAGCCACTGTCATAGCTTG	
pCF10oriTF3	GGTAAGTCGAAACGTCAAT	
pCF10oriTR1	CTCCTTAGTTTCGACAATTG	
pORIT-16-TriP-F	TAAAGCCTGGGGTGCCTAATGAG	
pORIT-16-TriP-R	AATACGCAAACCGCCTCTC	
TriP-pcfE-F	ATGGACCAATTAACGGACG	
TriP-pcfE-R	CCCATCGCTACACTTTGACAT	
TriP-pcfF-F	GCGCGTCCTATTCAAAGAATAG	
TriP-pcfF-R	TGAAACTGATTGGCCAGACGG	
GSTF5	CGGGATCCCATATGGAGAATAAACAAAAACTAAAA	
GSTF3	CGGAATTCTTACGATTGATCCTTTCTCT	
BspHI-pcfC	ATGCTCATGACACAGACGTACAAAAAAGAACTG	
RBS-C	CGGGATCCTTAAAGGAGGTATTATCATATGGCTCGTTTTGCTACACC TGCT	
ΔN103R	ACATGCATGCCTGCAGCTCGAGTTAAACGTGTGTTTCTTCTT	
pCF10 oriT-Sense	AAATTCGCAACATGCTAGCATGTTGCTCCGCTTGCAAAAAGAAA GCCG	
pCF10 oriT-AntiSense	GATCCGGCTTTCTTTTTGCAAGCGGAGCAACATGCTAGCATGTTGCG	

were resuspended in 5 ml of buffer A (20 mM Tris-HCl [pH 8.0], 0.25 M NaCl, 1× EDTA-free protease inhibitor cocktail [Roche]) and sonicated to clarity. Cell lysates were centrifuged at 15,000 × *g* at 4°C for 20 min, and the supernatants were subjected to an affinity column by using Talon (Co^{2+}) resin (Clontech) equilibrated with buffer A. Bound proteins were incubated with Talon agarose at 4°C for 40 min, washed extensively with buffer A containing 20 mM imidazole, and eluted with buffer A containing 200 mM imidazole.

The pooled fractions with high purity (>90%) were further purified and analyzed by gel filtration chromatography. For large sample preparations, HiPrep 16/60 Sephacryl S200 HR columns were used with AKTA systems (GE Healthcare). The columns were preequilibrated and run with buffer B (50 mM Tris-HCl [pH 7.5], 1 mM dithiothreitol, 1 mM EDTA, 100 mM KCl, 5% glycerol). For analytical gel filtration, a Tricorn high-performance column (Superdex 75 10/300 GL) was preequilibrated and run with buffer C (50 mM HEPES [pH 7.0], 100 mM NaCl, 2 mM $MgCl_2$, 0.1 mM EDTA, 5% glycerol). The gel filtration columns were calibrated by using aldolase, albumin, chymotrypsinogen A, and RNase A (GE Healthcare) as standards.

Purified His_6-PcfCΔN103 was sent to Cocalico Biologicals, Inc., (Reamstown, PA) for antibody production in New Zealand White rabbits as previously described (40). Similarly, purified His_6-PcfF and PcfG-His_6 were used to raise antibodies in New Zealand White rabbits. Anti-PrgB antibodies were generated previously (54).

PcfC, PcfF, and PcfG interaction assays. *E. faecalis* cells carrying pCF10 or pCF10Δ*pcfC* (20 ml) were induced with 20 ng/ml cCF10 pheromone peptide for 1.5 h, and cells were lysed by incubation at 4°C for 3 h in lysis buffer (20 mM Tris-HCl [pH 8.0], 150 mM NaCl, 1× protease inhibitor cocktail, 1% Triton X-100). The lysate was centrifuged at 4°C for 30 min, and the soluble material was mixed with Talon resin alone or prebound with PcfG-His_6 or His_6-PcfF. After incubation at 4°C for 3 h, the resins were washed extensively with buffer A with 20 mM imidazole, and bound proteins were eluted with buffer A containing 250 mM imidazole. Eluted fractions were assayed for PcfC, PcfF, and PcfG proteins by SDS-PAGE and immunostaining.

For glutathione *S*-transferase (GST) affinity chromatography, soluble fractions of *E. coli* cells producing GST-PcfCΔN103, GST-PcfCΔN103K156T, or GST alone were mixed with 50 μl of glutathione-Sepharose beads for 1 h at room temperature (RT). The Sepharose beads were pelleted by centrifugation at 500 × *g* for 5 min and washed three times with 1× PBS. The beads were resuspended in 500 μl of binding buffer (20 mM Tris-HCl [pH 8.0], 0.1 M NaCl, 10 μg bovine serum albumin). Purified PcfG-His_6 or His_6-PcfF (20 μg) prepared as described above was incubated with the glutathione-Sepharose beads alone or prebound with GST or the GST-PcfC fusion proteins for 3 h at RT. The beads were pelleted and washed five times with 1 ml of binding buffer containing 0.1% Triton X-100. The extensively washed Sepharose beads were eluted twice with elution buffer (10 mM glutathione, 0.1 M NaCl). The eluates were analyzed by SDS-PAGE and immunostaining.

TNP-ATP binding assay. His_6-PcfCΔN103 binding to the fluorescent ATP analog TNP-ATP (Molecular Probes, Inc.) was determined by fluorescence emission with a F-2000 fluorescence spectrophotometer as previously described (36, 39, 62). Briefly, purified protein (2 μM) obtained by sequential affinity and gel filtration chromatographies was mixed with TNP-ATP (30 μM) in Tris buffer (20 mM Tris-HCl [pH 8.0] and 50 mM NaCl in a 2-ml final volume). Following incubation at RT for 10 s, the fluorescence emission spectrum between 470 and 650 nm was monitored upon excitation at 410 nm. For titration studies, TNP-ATP was added sequentially to a fluorescence cuvette containing 1.5 μM of protein. The background intrinsic fluorescence of TNP-ATP in Tris buffer was also measured and subtracted from fluorescence values obtained for the TNP-ATP–protein mix.

TrIP assay. The transfer DNA immunoprecipitation (TrIP) assay was carried out essentially as previously described (16) with modifications as follows. A 10-ml culture of pheromone-induced cells in mid-exponential phase was pelleted and resuspended in 2.5 ml 10 mM sodium phosphate buffer (pH 7.0). Formaldehyde (FA) was added at a final concentration of 1%, and cells were incubated at 37°C for 30 min. Glycine was added at a final concentration of 125 mM, and cells were incubated at RT for 10 min and washed twice with 5 ml 1× PBS (pH 7.3). Cells were converted to protoplasts by incubation in lysozyme solution as described above, and protoplasts were lysed by incubation in immunoprecipitation buffer (20 mM Tris-HCl [pH 8.0], 150 mM NaCl, 1 mM EDTA, 10 mg lysozyme, 1× protease inhibitor cocktail, 0.5% Triton X-100) for 20 min at 37°C and sonication (Branson). The supernatant from subsequent centrifugation was incubated with protein A-Sepharose CL4B (Pharmacia) (30-μl bed volume) for 60 min at RT and centrifuged at 5,000 × *g* to remove protein A-Sepharose and nonspecifically bound proteins. The supernatant was incubated overnight at 4°C with antibody coupled to Protein A-Sepharose CL4B. The supernatant after this step corresponds to the soluble fraction. The beads were washed twice with NP1 buffer supplemented with 1% Triton X-100 and once with NP1 buffer supplemented with 0.1% Triton X-100. To reverse the FA cross-links, immunoprecipitates were resuspended in 150 ml of elution buffer (50 mM Tris-HCl [pH 8.0], 10 mM EDTA, 1% SDS) and incubated overnight at 65°C. Supernatants were treated at 37°C for 2 h with 150 μl of 60 mM Tris-HCl (pH 6.8), 5% glycerol, and proteinase K (100 μg/ml). The DNA was purified by phenol-chloroform extraction, precipitated with isopropanol, and washed with 70% ethanol. Immunoprecipitated DNA was resuspended in 25 ml of Tris-EDTA and subjected to PCR amplification as described previously (16). For DNA detection, primers were designed to amplify a 315-bp region of pCF10, a 175-bp region of pOriT, and a 485-bp region of the chromosome.

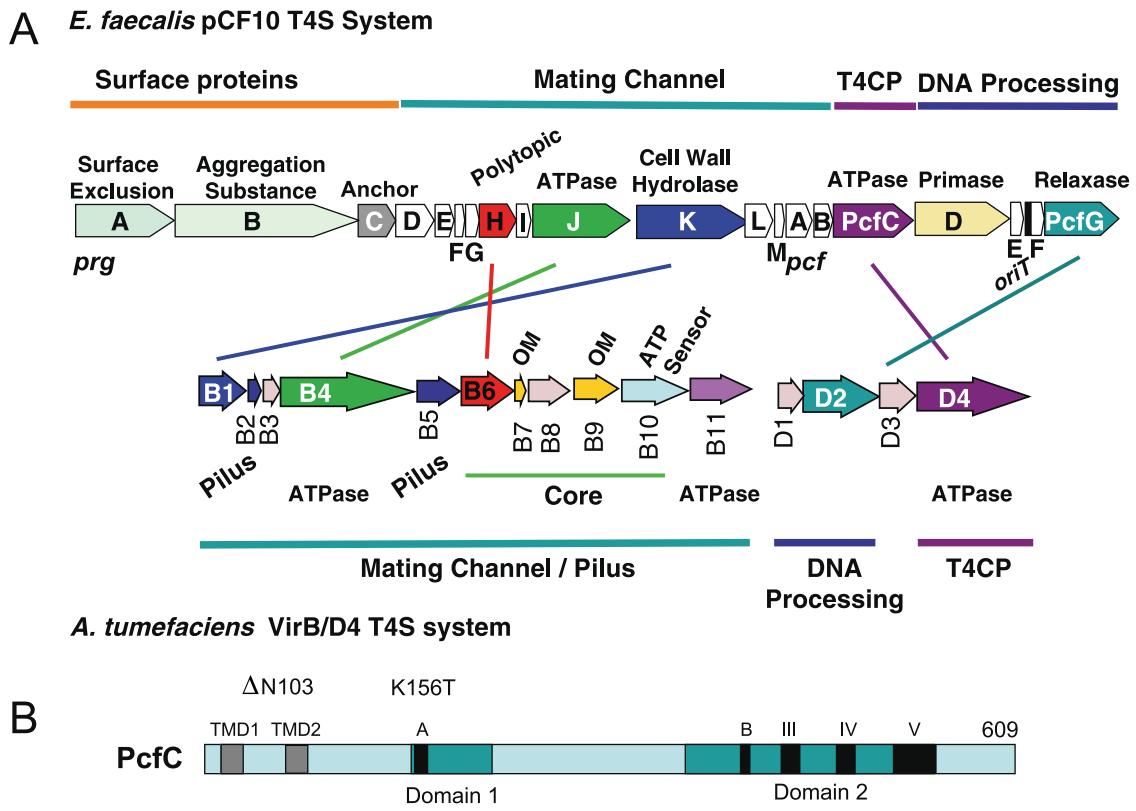

FIG. 1. pCF10 Tra region gene arrangement, protein functions, and similarities with the *Agrobacterium tumefaciens* VirB/D4 T4S system. (A) The *prg* and *pcf* genes are grouped according to proposed functions and are color matched with genes encoding VirB/D4 protein homologs. Core, genes whose products form a stable subassembly and are widely conserved among gram-negative T4S systems (20). The four related Prg/Pcf and VirB proteins exhibit between 18 and 25% sequence identities. (B) PcfC resembles T4CPs of gram-negative T4S systems in its domain architecture, with putative TM domains (TMDs) (gray); domains 1 and 2 (aqua); and conserved motifs (black), including Walker A and B NTP binding motifs (60). The locations of the two PcfC mutations (ΔN103, K156T) characterized in these studies are shown.

EMSA. Single-stranded DNA (ssDMA) and double-stranded DNA (dsDNA) substrates were prepared as follows. The dsDNA substrate was constructed by PCR amplification of a 186-bp fragment of pCF10 encompassing the *oriT* sequence by use of the primer pair pCF10oriTF3/pCF10oriTR1 and pCF10 as the template and purification with the QIAquick PCR purification kit (Qiagen). ssDNA substrates included pCF10-S, which contains the sense-strand sequence of the minimal pCF10 *oriT*, and pCF10-AS, which contains the corresponding antisense-strand sequence. Both oligonucleotides were synthesized and purified by high-pressure liquid chromatography and PAGE. (Advanced Genetic Analysis Center and Microchemical Facility, University of Minnesota). ssDNA and dsDNA substrates were labeled at the 3′ ends with digoxigenin (DIG)-11-ddUTP with the DIG gel shift kit (Roche) according to the manufacturer's instructions. A 39-mer DIG-labeled dsDNA oligonucleotide (supplied with the DIG gel shift kit) served as a non-*oriT* substrate. Electrophoretic mobility shift assays (EMSAs) were carried out in 20-μl reaction mixtures composed of recombinant proteins, DIG-labeled ssDNA or dsDNA, 0.2 μg of poly[d(A-T)], 0.1 μg of poly-L-lysine, 1× reaction buffer (20 mM Tris HCl [pH 8.0], 0.1 M KCl, 10% glycerol, 5 mM EDTA). The reaction mixtures were incubated at RT for 15 min, loaded onto 8% polyacrylamide gels in 0.5× Tris-borate-EDTA buffer (pH 7.9), and then subjected to electrophoresis at 100 V for 1.5 h and electrotransfer to a nylon membrane (Roche) at 6 V for 2 h with the Genie electrophoretic blotter (Idea Scientific). DIG-labeled DNA was visualized by an enzyme immunoassay (DIG gel shift kit; Roche) following the manufacturer's instructions. In competitive EMSAs, a molar excess (10- or 100-fold) of cold competitor DNA was added to the preformed probe-protein complexes (18).

Microscopy and image analysis. *E. faecalis* cells were grown to exponential phase and induced with 20 ng/ml of cCF10 for 1.5 h or incubated for this period without induction. Equivalent amount of cells (optical density at 600 nm = 1.0) were pelleted, washed three times with PBS, and resuspended in 300 μl 1× PBS. Cells were examined by immunofluorescence microscopy (IFM) as described previously (2) with minor modifications. Briefly, 20 μl of cells was spotted on 0.1% poly-L-lysine-treated microscopic slides, fixed overnight, and then treated with lysozyme solution (10 mM Tris-HCl [pH 8.0], 50 mM NaCl, 1 mM EDTA, 20% sucrose, 15 mg/ml lysozyme) at RT for 30 min. Permeabilized cells were analyzed with anti-PcfC, PcfF, -PcfG, and -PrgB primary antibodies and Alexa Fluor 488 goat anti-rabbit immunoglobulin G secondary antibody (Molecular Probes). Images of cells were acquired with an Olympus BX60 microscope equipped with a 100× oil immersion phase-contrast objective as described previously (2).

RESULTS

pCF10 T4S gene arrangement and features. The putative *tra* region of pCF10 encompasses up to 20 open reading frames divisible into three functional groups (Fig. 1A). At the beginning of the gene cluster are *prg* genes encoding surface proteins PrgA (surface exclusion), PrgB or AS (cell-cell adhesion), and PrgC (unknown function). Next, 13 *prg/pcf* genes are postulated to encode the mating pair formation (Mpf) channel subunits; these genes code for (i) four homologs of gram-negative T4S systems (with the *A. tumefaciens* VirB/D4 system (21) as a reference, PrgH [29 kDa; polytopic VirB6-like channel subunit], PrgJ [85 kDa; VirB4-like ATPase], PrgK [99 kDa; VirB1-like cell wall hydrolase], and PcfC [70 kDa; VirD4-like ATPase], (ii) other proteins with one or more putative α-helical TM domains (PrgD, PrgF, PrgI, PrgL), and (iii) predicted cytoplasmic proteins (PrgE, PrG, PrgM, PcfA, and PcfB). As expected, this region lacks the components of gram-negative

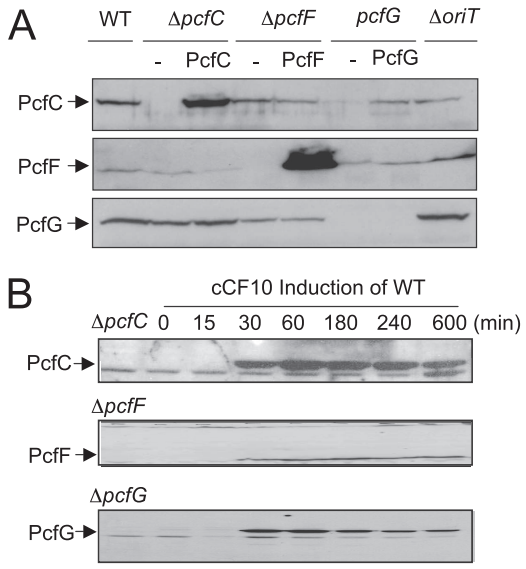

FIG. 2. Synthesis of PcfC, PcfF, and PcfG in WT and mutant strains. (A) Detection of Pcf proteins in mutant strains listed at top without (−) or with synthesis of the complementing protein. Immunoblots were developed with antibodies to the proteins listed at left. For comparisons, total protein extracts were loaded on a per-cell equivalent basis. Proteins were synthesized from the constitutive promoter P_{23} (PcfC and PcfF) or inducible promoter P_{nis} (PcfG). PcfG synthesized from the weak promoter P_{nis} accumulated at levels detectable only upon enrichment of the membrane fraction (data not shown). (B) Steady-state levels of PcfC, PcfF, and PcfG in strain CK104(pCF10) (WT) were assessed over time following induction with peptide pheromone cCF10. Left lanes, immunoreactive material from the mutant strains shown.

systems thought to bridge inner and outer membrane machine subassemblies (e.g., *A. tumefaciens* VirB8 and VirB10 energy sensor), associate with the outer membrane (VirB7 lipoprotein and VirB9), or elaborate the conjugative pilus (VirB2 and VirB5). This region encodes a VirB4-like putative ATPase, characteristic of all T4S systems identified to date, and does not encode a VirB11 homolog, a third ATPase subunit of most but not all T4S systems (61). At the distal end of the *tra* region are the DNA transfer and replication (Dtr) genes whose products assemble as the catalytically active relaxosome at *oriT*. These include PcfF and PcfG relaxase, both essential for processing, and PcfD and PcfE, the production of which enhances plasmid transfer frequencies by approximately 10- and 60-fold, respectively (18).

Overall, the putative substrate receptor PcfC shares limited sequence similarities with the well-characterized gram-negative T4CPs, e.g., *A. tumefaciens* $VirD4_{At}$, RP4 $TraG_{RP4}$, R388 $TrwB_{388}$ (the subscript designates species or plasmid origin) (Fig. 1B). However, PcfC possesses all conserved domains and motifs previously identified and shown to be functionally important for the gram-negative T4CPs. These include two N-terminal TM domains flanking a predicted periplasmic loop, Walker A and B NTP binding motifs, and three additional motifs clustered in a larger region previously designated domain 2 (Fig. 1B) (60).

***pcfC* genetic complementation and PcfC, PcfF, and PcfG protein accumulation.** We assessed the effect of a Δ*pcfC* mutation on pCF10 plasmid transfer. Upon pheromone induction, the Δ*pcfC* mutant strain accumulated wild-type (WT) levels of PcfF and PcfG, indicating that the Δ*pcfC* is nonpolar on expression of downstream genes (Fig. 2A). This strain failed to transfer the mutant plasmid even in overnight matings on a solid agar surface (Table 2). For genetic complementation tests, WT *pcfC* was expressed from the nisin-inducible promoter P_{nis} on plasmid pSM3545 or from the constitutive promoter P_{23} on pCIp23. Interestingly, PcfC accumulated at high levels when synthesized from the P_{23} promoter (Fig. 2A) but at a level detectable only by concentration of cellular fractions when synthesized from P_{nis} (see Fig. 3C). Yet, *pcfC* expression from both promoters on plasmid pCY25 (P_{23}-*pcfC*) or pCY24 (P_{nis}-*pcfC*) restored plasmid transfer to near-WT levels (Table 2), which indicates that PcfC is not rate limiting for plasmid transfer when synthesized at low levels.

We constructed two PcfC mutants for further study, one with Thr substituted for the invariant Lys residue in the Walker A motif (K156T) and a second deleted of the N-terminal putative membrane-spanning domain (ΔN103) (Fig. 1B). The mutant proteins accumulated at detectable levels (see below), but neither supported pCF10Δ*pcfC* transfer when synthesized from pCY28 (P_{23}-*pcfCK156T*) or pCY31 (P_{23}-*pcfC*Δ*N103*) (Table 2), showing that both of these PcfC motifs are essential for pCF10 transfer. Merodiploid strains cosynthesizing native PcfC from pCF10 and the mutant proteins from pCY28 or pCY31 transferred pCF10 at slightly reduced frequencies compared to the corresponding vector-only isogenic strains (Table 2), consistent with the idea that PcfC functions as a homo- or heteromultimer.

We also assayed for effects of Δ*pcfC*, Δ*pcfF*, and *pcfG* mutations and a Δ*oriT* mutation, made by deleting a ~400-bp intergenic region between *pcfE* and *pcfF* (Fig. 1A), on pheromone-inducible accumulation of PcfC, PcfF, and PcfG. In induced cells, Δ*pcfC*, Δ*pcfF*, *pcfG*, and Δ*oriT* mutations generally had little or no effect on accumulation of the other two Pcf proteins, with the interesting exception that the *pcfG* mutant accumulated PcfC at very low levels and the mutant expressing *pcfG* in *trans* accumulated PcfC at high levels, suggestive of a possible stabilizing effect of the relaxase on the T4CP (Fig. 2A).

TABLE 2. Transfer frequencies of WT pCF10 and mutant derivatives

Plasmid(s)[a]	Transfer frequency (transconjugants/donor)[b]
pCF10	1.7×10^{-1}
pCF10Δ*pcfC*	$<10^{-8}$
pCF10Δ*pcfC*, pCY25 (P_{23}-*pcfC*)	8.9×10^{-3}
pCF10Δ*pcfC*, pCY28 (P_{23}-*pcfCK156T*)	$<10^{-8}$
pCF10Δ*pcfC*, pCY31 (P_{23}-pcfCΔN103)	$<10^{-8}$
pCF10Δ*pcfC*, pCY24 (P_{nis}-*pcfC*) + nisin	4.1×10^{-2}
pCF10Δ*pcfC*, pCY24 (P_{nis}-*pcfC*) − nisin	2.6×10^{-6}
pCF10, pCY28[c] (P_{23}-*pcfCK156T*)	3.77×10^{-2}
pCF10, pCY31[c] (P_{23}-*pcfC*Δ*N103*)	8.11×10^{-2}

[a] Donor strain, CK104; recipient strain, OG1SSP or OG1ES.
[b] Experiments were repeated three times in triplicate, and a representative experimental result is reported.
[c] Isogenic strains carrying pCF10 and pCY25 (P_{23}-*pcfC*) or the P_{23} vector plasmid pCIp23 or pDL278p23 displayed WT pCF10 transfer frequencies (data not shown).

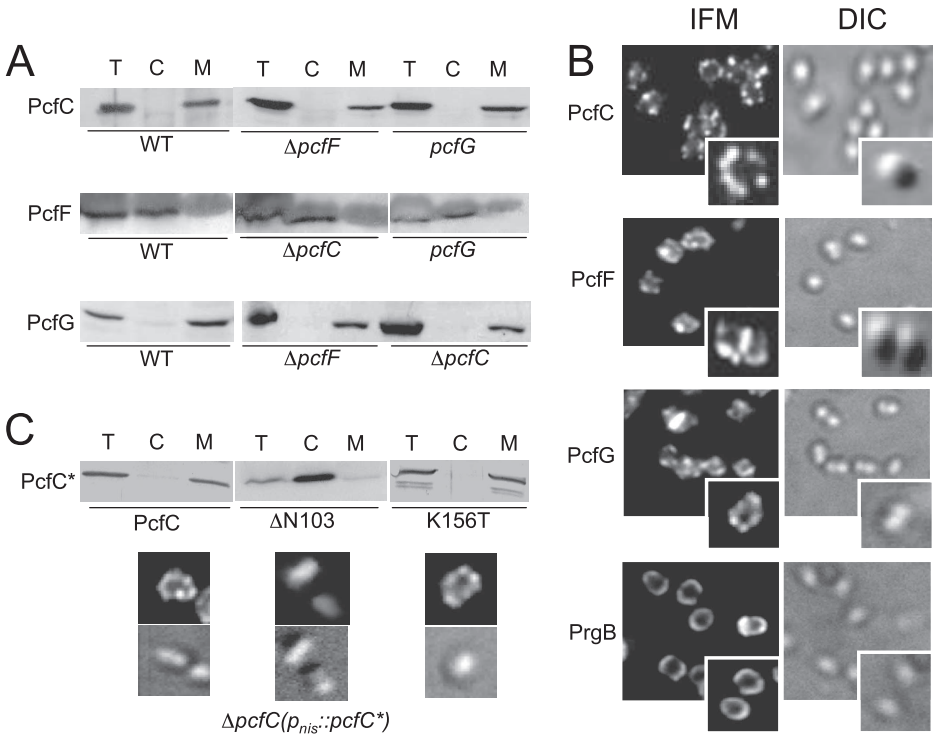

FIG. 3. Subcellular locations of PcfC, PcfF, and PcfG. (A) Pcf proteins in total cell (T), cytoplasm (C), and membrane (M) fractions of cCF10-induced CK104(pCF10) (WT) or the mutant strains listed below each panel. Immunoblots were developed with antibodies to the proteins listed at left. (B) Spatial distribution of PcfC, PcfF, PcfG, and PrgB proteins in pheromone-induced CK104(pCF10) cells. Proteins were detected by IFM with antibodies to the proteins listed at the left. Corresponding cells were visualized by Nomarski microscopy (differential interference contrast [DIC]). For each protein, representative fields with multiple cells or magnified individual cells are shown. (C) Corresponding subcellular fractionation (using 20× concentrated fractions) and spatial analyses of PcfC and PcfCΔN103 and PcfCK156T mutant proteins synthesized from the P_{nis} promoter in the Δ*pcfC* mutant background.

WT cells show a burst in plasmid transfer within 15 min postinduction and a subsequent rapid increase to peak levels within ~2 h postinduction. Cells then enter a 2- to 3-h decline phase marked by a reduction in plasmid transfer to preinduction levels (38). Correspondingly, PcfC, PcfF, and PcfG were undetectable in uninduced cells and accumulated rapidly within 15 to 30 min following induction, and then levels of all three proteins remained high throughout the period of robust plasmid transfer (Fig. 2B). However, levels of all three proteins remained unchanged or decreased only slightly up to 10 h postinduction, well after conjugation frequencies had declined to preinduction levels (Fig. 2B) (38). Synthesis of PcfC, PcfF, and PcfG therefore is essential for pCF10 transfer, but targeted degradation of these transfer factors most probably does not account for the significant reduction in plasmid transfer over prolonged induction periods.

Subcellular localization and spatial positioning of PcfC, PcfF, and PcfG. Cellular localization studies of T4S machines and cognate substrates have proven valuable for understanding the requirements for and dynamics of T4S-mediated substrate recruitment and binding in vivo (2, 4). Initially, we determined the subcellular localization of PcfC, PcfF, and PcfG by fractionation of WT cells. As expected from its secondary structure predicting a transmembrane topology, PcfC fractionated with the membrane of pheromone-induced cells (Fig. 3A) and was partially extracted from membranes with Triton X-100 and other nonionic detergents but not with treatments including salt, high pH, and bicarbonate (data not shown). PcfF and PcfG do not carry predicted TM domains, and although PcfF fractionated predominantly with the cytoplasmic material, PcfG partitioned almost exclusively with the WT cell membrane (Fig. 3A). Nonionic detergents, e.g., Triton X-100, 1 M NaCl, and bicarbonate, released a substantial amount of PcfG from the membrane (data not shown), suggestive of a peripheral membrane association. We further asked whether these fractionation patterns were altered in the Δ*pcfC*, Δ*pcfF*, and *pcfG* mutant backgrounds (Fig. 3A). PcfC partitioned with the membrane fractions of both Δ*pcfF* and *pcfG* mutant strains, and PcfG similarly displayed WT fractionation behavior in the Δ*pcfC* mutant. Thus, both the putative T4CP and the relaxase bind the membrane independently of each other.

Next, we analyzed the spatial organization of PcfC, PcfF, and PcfG in pheromone-induced WT cells by IFM. Interestingly, each protein formed ca. two to six punctate foci at the peripheries of nearly all pheromone-induced WT cells (Fig. 3B). Moreover, each Pcf protein displayed WT distribution patterns in mutant strains lacking one of the other Pcf proteins (data not shown). In control experiments, no puncta were visible at the peripheries of uninduced WT cells or induced Δ*pcfC*, Δ*pcfF*, and *pcfG* mutant strains using antibodies against the missing protein (data not shown). Because of the small size of *E. faecalis* cells and the limits of resolution of IFM, we could

not confirm whether PcfC, PcfF, and PcfG colocalize at the WT cell envelope. However, the results of in vitro protein-protein interaction studies described below are consistent with this proposal.

In further studies (Fig. 3C), we found that PcfCΔN103 deleted of the N-terminal putative TM domain partitioned almost exclusively with the cytoplasmic fraction, whereas the PcfCK156T Walker A mutant displayed a WT fractionation pattern. Correspondingly, PcfCΔN103 displayed uniform fluorescence consistent with a cytoplasmic distribution, whereas PcfCK156T formed WT foci at cell peripheries. The N-terminal domain therefore mediates membrane binding and spatial organization of PcfC, whereas the K156T mutation does not appear to disrupt PcfC function through effects on membrane binding.

Finally, we compared the spatial organization of PcfC, PcfF, and PcfG with that of the AS PrgB. In early electron microscopy studies, it was shown that PrgB distributes uniformly at the polar caps in most cells and as a narrow band approximately at the midcell in a fraction of other cells (54). Similarly, when assessed by IFM, PrgG distributed uniformly at the polar caps of most cells (Fig. 3B). We did not detect any punctate foci reminiscent of those formed by PcfC, PcfF, and PcfG at any time throughout a 10-h induction period, confirming that T4S processing/transfer factors and the surface adhesin AS differ distinctly in their spatial organization at the *E. faecalis* envelope.

PcfC binds the processed form of pCF10 in vivo. The observed similarities in PcfC, PcfF, and PcfG spatial patterns suggested the possibility that PcfC binds the pCF10 transfer intermediate in vivo. We tested for such an interaction by TrIP, adapted from the chromatin immunoprecipitation assay (45), for detection of substrate DNA-T4S channel subunit contacts (3, 16). As shown in Fig. 4A, anti-PcfC antibodies precipitated pCF10 DNA from extracts of FA-treated OG1RF(pCF10) cells. In control experiments, the anti-PcfC antibodies did not precipitate detectable amounts of chromosomal DNA from extracts of FA-treated OG1RF(pCF10) cells or of plasmid or chromosomal DNA from non-FA-treated OG1RF(pCF10) cells or the FA-treated isogenic Δ*pcfC* mutant (Fig. 4A). Further, the anti-PcfC antibodies precipitated pOriT, a heterologous vector plasmid (pDL278) engineered to carry the pCF10 *oriT* sequence, but not a coresident pCF10Δ*oriT* mutant plasmid. The antibodies also did not precipitate detectable levels of the vector plasmid alone. We also assayed for, but did not detect, precipitation of *pcfG* and Δ*oriT* mutant plasmids from extracts of FA-cross-linked strains (Fig. 4B). Thus, pCF10 processing at *oriT* is required for detectable pCF10-PcfC binding, indicating that PcfC binds exclusively to the pCF10 transfer intermediate and not the closed covalent circular form of the plasmid in vivo.

Finally, we tested for the capacity of the PcfCΔN103 and the PcfCK156T Walker A mutant proteins to bind the pCF10 substrate. As shown in Fig. 4C, the anti-PcfC antibodies precipitated pCF10 but not chromosomal DNA from extracts of FA-treated strains producing both mutant proteins. PcfC therefore retains the ability to interact with the pCF10 substrate in vivo independently of its N-terminal domain or an intact Walker A motif.

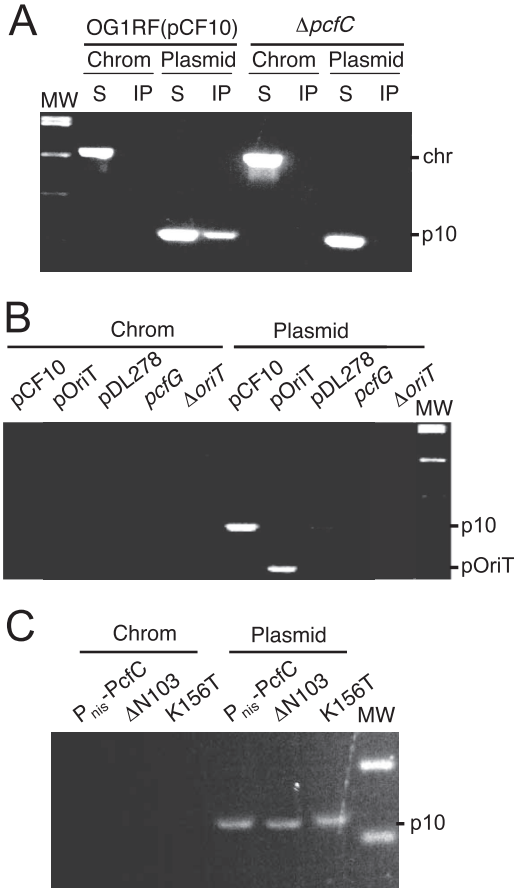

FIG. 4. Detection of the PcfC-pCF10 interaction in vivo by use of the TrIP assay. (A) Detection of pCF10 or chromosomal DNA in immunoprecipitates recovered from FA-treated OG1RF(pCF10) or the isogenic Δ*pcfC* mutant cell extracts with anti-PcfC antibodies. PCR amplification products were generated with primers against a pCF10 gene fragment (listed as plasmid [top] or p10 [right]) or a chromosomal fragment (Chrom [top] or chr [right]). MW, molecular mass markers. PCR products were generated using supernatant (nonprecipitated) (S) and immunoprecipitated (IP) material. (B) Detection of PCR-amplified pCF10 or PoriT (plasmid [top] or p10 or pOriT [right]) or chromosomal (Chrom) DNA in immunoprecipitates recovered from FA-treated OG1RF carrying the plasmids listed. (C) Detection of PCR-amplified pCF10 (plasmid [top] or p10 [right]) or chromosomal (Chrom [top]) DNA in immunoprecipitates recovered from FA-treated strains carrying pCF10Δ*pcfC* and plasmids producing native PcfC, PcfCΔN103, or PcfCK156T from promoter P_{nis}.

PcfC binds ssDNA and dsDNA in vitro. The results of the TrIP assays described above supplied evidence for binding of the pCF10 transfer intermediate in vivo but did not establish whether PcfC exhibits DNA sequence specificity or interacts with the PcfF or PcfG processing factors. We attempted to purify PcfC for further biochemical analyses but were unable to obtain a soluble form of the full-length protein. However, soluble His-tagged PcfCΔN103 was readily overproduced in *E. coli* and purified to >95% homogeneity through sequential steps of Co^{2+} affinity and size exclusion chromatographies (Fig. 5A). His_6-PcfCΔN103 eluted from the size exclusion column as a narrow peak with an estimated molecular size of 60 kDa, the expected size of the monomer.

His_6-PcfCΔN103 bound both dsDNA and ssDNA *oriT*-con-

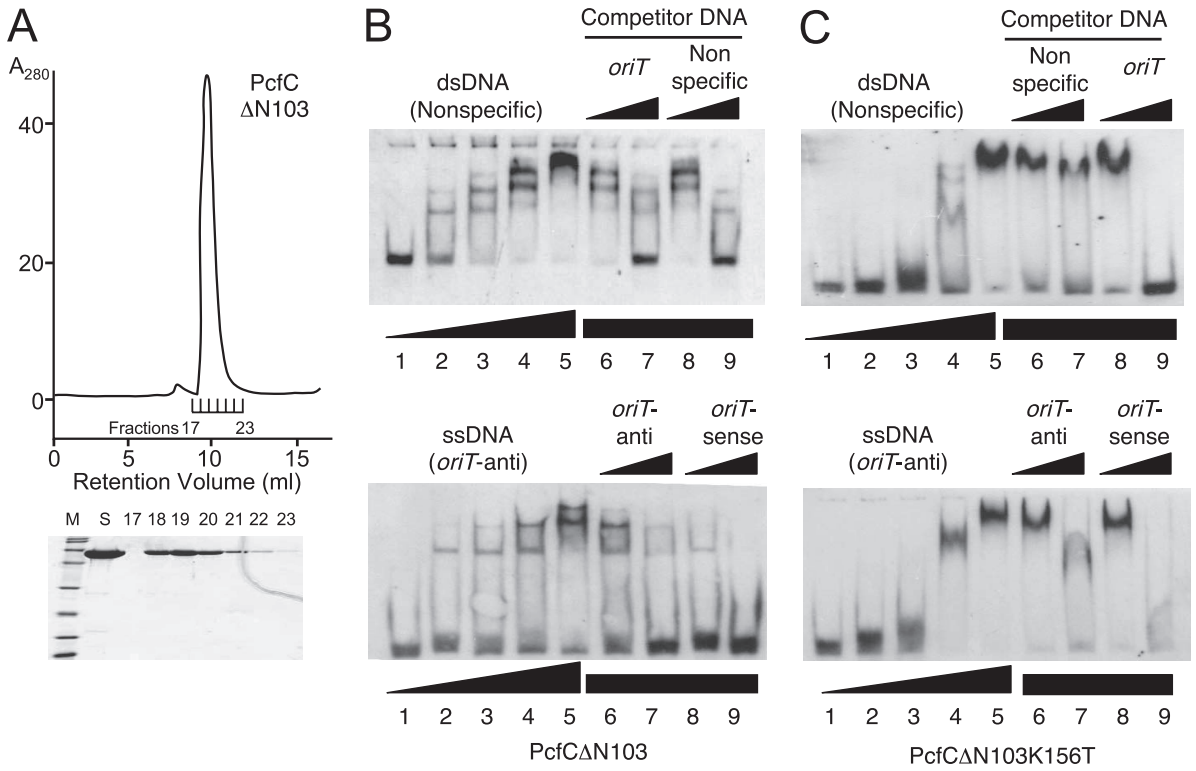

FIG. 5. His_6-PcfCΔN103 purification and DNA binding in vitro. (A) Recombinant His_6-PcfCΔN103 was purified by sequential affinity and gel filtration chromatographies (see text). Upper panel, gel filtration elution profile showing protein in peak fractions corresponding to a molecular size of ~60 kDa. Lower panel, Coomassie blue-stained gel showing relative amounts of PcfC protein in the fractions listed. (B) DNA binding activities of His_6-PcfCΔN103 assessed by EMSA. Upper panel, EMSA using the 3′-end-DIG-labeled 39-mer dsDNA fragment lacking the *oriT* sequence (nonspecific DNA; 16 fmol). Lane 1, DNA probe only. Lanes 2 to 9, DNA probe plus His_6-PcfCΔN103 at the following concentrations: 2, 83 nM; 3, 166 nM; 4, 332 nM; 5 to 9, 498 nM. Lanes 6 and 7, protein was preincubated with unlabeled *oriT*-containing competitor dsDNA at concentrations 10-fold and 100-fold higher than that of the DIG-labeled substrate. Lanes 8 and 9, protein was preincubated with unlabeled competitor nonspecific DNA at concentrations 10-fold and 100-fold higher than that of the DIG-labeled substrate. Lower panel, EMSA using the 3′-end-DIG-labeled *oriT*-antisense ssDNA fragment (nonspecific DNA; 30 fmol). Reaction conditions were the same as described for the upper panel. (C) EMSA using purified His_6-PcfCΔN103K156T. Panels and reaction conditions are same as described for panel B.

taining substrates, as shown by retardation of labeled DNA in polyacrylamide gels (Fig. 5B). For both substrates, shifted complexes increased in their molecular sizes as a function of PcfC protein concentration, suggesting that PcfC monomers bind DNA substrates noncooperatively at multiple sites or multimerize or aggregate on DNA at high protein concentrations. Complex formation was inhibited by unlabeled *oriT*-containing and nonspecific competitor DNAs, indicating that PcfC binds both dsDNA and ssDNA substrates without sequence specificity. In further experiments, additions of NTPs to the reaction mixtures did not cause detectable changes in DNA binding activities (data not shown). Finally, consistent with results of the TrIP assay, His_6-PcfCΔN103 carrying a K156T mutation bound the DNA substrates (Fig. 5C). Some differences in band shift patterns were detected between the His_6-PcfCΔN103 and K156T mutant protein (compare Fig. 5B and C), possibly reflecting a slightly reduced affinity of the K156T mutant for DNA or a propensity of the mutant protein to aggregate in solution.

PcfCΔN103 binds TNP-ATP. We assayed for NTP binding and hydrolysis activities of purified His_6-PcfCΔN103, the former with TNP-ATP, a fluorescent ATP analog that exhibits enhanced fluorescence when bound to macromolecules (36, 39, 62). His_6-PcfCΔN103 bound the fluorescent ATP analog, as did the purified K156T mutant derivative albeit with a slightly reduced affinity (Fig. 6A). By analysis of the binding curves, His_6-PcfCΔN103 bound TNP-ATP with a dissociation constant (K_d) of 0.41 μM and the K156T mutant with a K_d of 0.57 μM (Fig. 6B). Thus far, we have not been able to show that purified His_6-PcfCΔN103 hydrolyzes ATP or other NTPs in vitro.

PcfC interacts with the relaxosome components PcfF and PcfG. In view of its nonspecific DNA binding activity, we postulated that PcfC recognizes the pCF10 substrate through interactions with one or more relaxosome components. To test this possibility, we purified His_6-tagged forms of PcfF and PcfG and assayed for interactions with full-length PcfC and PcfCΔN103. Recombinant His_6-PcfF from *E. coli* was soluble and could be purified in large amounts by sequential affinity and size exclusion chromatographies (Fig. 7A). The ~14-kDa protein eluted from the latter column as a single sharp peak corresponding to a ~60-kDa species, most probably a tetramer. PcfG-His_6 forms inclusion bodies when produced in *E. coli*, but small amounts of soluble relaxase could be purified to >90% homogeneity by Co^{2+} affinity chromatography (Fig. 7A).

His_6-tagged PcfF and PcfG were prebound to Co^{2+} affinity

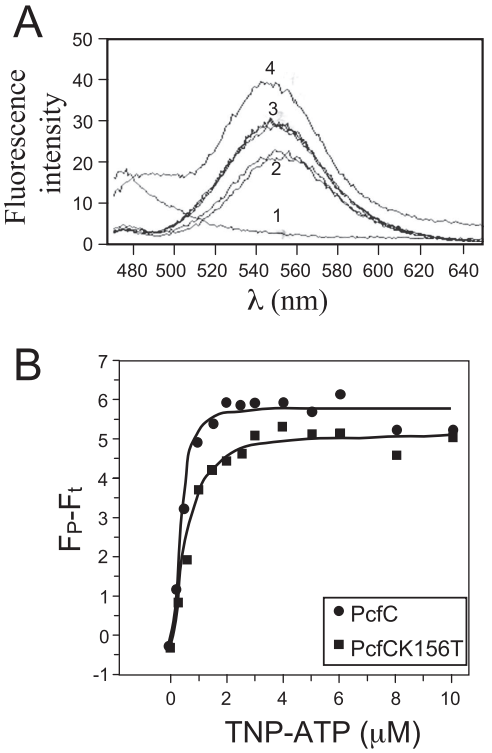

FIG. 6. His_6-PcfCΔN103 binds the fluorescent ATP analogue TNP-ATP. (A) Fluorescence was measured with an excitation wavelength of 410 nM and scanning wavelengths from 470 to 650 nM. Spectra 1 to 4 were taken from the following samples: 1, Purified His-PcfCΔN103 (2 μM) plus buffer; 2, TNP-ATP (30 μM) plus buffer (duplicate results are shown); 3, His-PcfCΔN103 (2 μM) plus TNP-ATP (30 μM) plus ATP (10 mM) (duplicate results are shown); 4, His-PcfCΔN103 (2 μM) plus TNP-ATP (30 μM). The spectrum obtained for His-PcfCΔN103K156T (2 μM) plus TNP-ATP (30 μM) closely matched that for His-PcfCΔN103 (data not shown). (B) Binding of TNP-ATP to WT and mutant PcfCΔN103. Concentration-dependent increases in TNP-ATP fluorescence in the presence of PcfCΔN103 (λ) and mutant K156T (*v*) (1.5 mM each) indicate binding of this ATP analog to PcfC. The apparent fluorescence (Fp − Ft) is represented in arbitrary units after subtraction of intrinsic TNP-ATP fluorescence in buffer alone. The solid lines show the best fit of the Hill model (Origin program), giving K_ds of 0.41 mM and 0.57 mM for WT PcfCΔN103 and mutant K151T, respectively.

resin and then incubated with Triton X-100-treated cell lysates of *E. faecalis* carrying pCF10 or pCF10Δ*pcfC*. Following extensive washing, proteins were eluted with imidazole and analyzed for the presence of the respective His-tagged protein and PcfC. As shown in Fig. 7B, His_6-tagged PcfF and PcfG bound PcfC present in pCF10-carrying cell extracts. PcfC did not bind the Co^{2+} resin in the absence of these His_6-tagged proteins and, additionally, the His_6-protein-bead complexes did not bind cross-reactive material migrating at the size of PcfC from Δ*pcfC* cell extracts (Fig. 7B).

Next, we purified a GST-tagged form of PcfCΔN103 from *E. coli* to assay for interactions with purified His_6-tagged PcfF and PcfG. GST-PcfCΔN103, or purified GST as a control, was prebound to the affinity resin and incubated with one of the His-tagged proteins. As shown in Fig. 7C, His_6-PcfF and PcfG-His_6 coeluted with GST-PcfCΔN103, but not with GST, upon incubation with glutathione. These data indicate that PcfC interacts directly with each of the processing factors, PcfF and PcfG.

Finally, we tested a prediction from previous studies (18) that PcfF interacts directly with PcfG in the absence of a DNA substrate. We constructed and purified GST-tagged PcfF and assayed as described above for binding to PcfG-His_6. As shown in Fig. 7D, PcfG-His_6 coeluted with GST-PcfF despite some apparent proteolysis at or near the GST fusion junction, indicative of a direct PcfF-PcfG interaction in vitro.

DISCUSSION

The pCF10 conjugation machine is an appealing gram-positive T4S system for detailed structure-function analysis due to its medical importance and rapid induction kinetics (38) (Fig. 2B), permitting detailed investigations of T4S machine assembly and function in space and time. Here, we used a combination of cytological and biochemical approaches to characterize the interface of the pCF10 processing and translocation reactions. The major findings from these investigations were as follows: (i) PcfC is essential for pCF10 transfer and requires both its N-terminal putative TM domain and an intact Walker A motif for function; (ii) PcfC, PcfF, and PcfG form punctate foci on the cell surface, whereas AS PrgB distributes uniformly mainly around the polar caps; and (iii) PcfCΔN103 and the K156T Walker A variant bind ATP, ss- and dsDNA, and the PcfF and PcfG processing factors in vitro, and native PcfC and the K156T mutant bind the processed form of pCF10 in vivo. These findings are discussed below in the context of a model in which the PcfF and PcfG processing factors and the PcfC substrate receptor interact at a few sites at the *E. faecalis* membrane to spatially coordinate early pCF10 processing and translocation reactions.

The pCF10 processing reaction. Previously, it was shown that purified PcfG catalyzes cleavage of an *oriT* ssDNA substrate in vitro but requires PcfF to bind and nick the corresponding dsDNA substrate (18). These findings suggested that PcfF recruits PcfG to the plasmid's *oriT* sequence, but they did not identify the underlying recruitment mechanism. The observations that both PcfF and PcfG assemble as punctate foci at the *E. faecalis* cell peripheries (Fig. 3) and that PcfF interacts directly with PcfG in vitro (Fig. 7) suggest PcfF binds the pCF10 *oriT* sequence and recruits PcfG through a direct protein-protein interaction to mediate relaxosome assembly at discrete sites at the cell envelope. PcfC also forms punctate foci (Fig. 3) and interacts in pairwise fashion with PcfF and PcfG in vitro (Fig. 7), which initially led us to consider that PcfC recruits one or both processing factors, or the assembled relaxosome, to the cell membrane as a means of coupling the processing and translocation reactions. However, this idea proved incorrect because PcfC, PcfF, and PcfG display WT spatial distribution patterns independently of each other or pCF10 DNA (Fig. 3; Y. Chen, unpublished data). Furthermore, with the TrIP assay we gained evidence that PcfC interacts exclusively with the processed form of pCF10 (Fig. 4). This requirement for DNA processing suggests that PcfC does not interact directly with the relaxosome but rather interacts with the transfer intermediate, provisionally comprised of PcfG covalently bound to the 5′ end of the T strand. Thus, we propose a sequence of events in which PcfF and PcfG assemble the

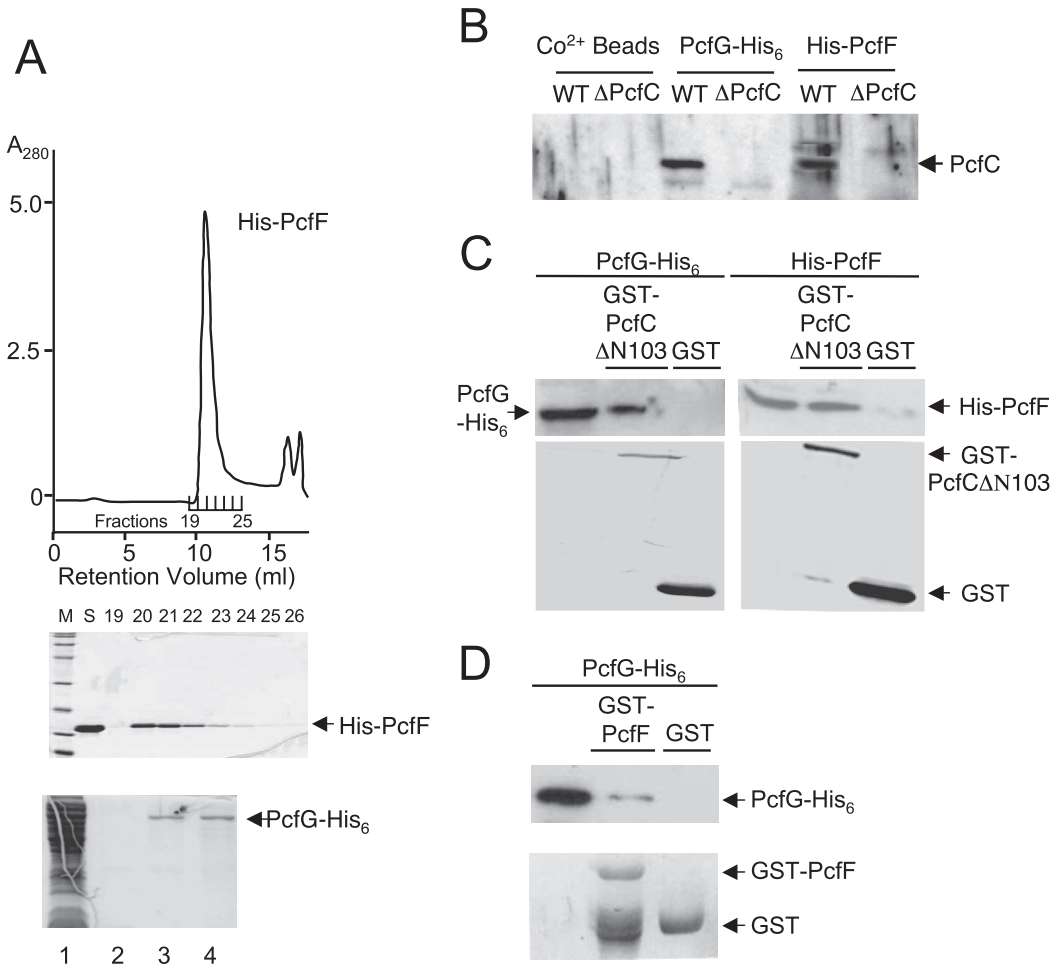

FIG. 7. His_6-PcfF purification, PcfG-His_6 enrichment, and in vitro protein-protein interactions. (A) Recombinant His_6-PcfF was purified by sequential affinity and gel filtration chromatographies (see text). Upper panel, gel filtration elution profile showing protein in peak fractions corresponding to a molecular size of ~60 kDa. Middle panel, Coomassie blue-stained gel showing relative amounts of His_6-PcfF protein in the fractions listed. Bottom panel, PcfG-His_6 enrichment by affinity chromatography. Lanes: 1, total extract from PcfG-His_6-producing *E. coli*; 2, final wash fraction; 3 and 4, first two fractions upon elution with 150 mM imidazole. (B) Binding of native PcfC to His-PcfF and PcfG-His_6-CO^{2+} bead complexes. His-tagged proteins prebound to the CO^{2+} beads were mixed with *E. faecalis* cell extracts, and PcfC bound to the Pcf protein-bead complexes was identified as described in the text. (C) Pull-down assays using purified His-tagged PcfF and PcfG and GST-tagged PcfCΔN103. (D) Pull-down assays using purified PcfG-His_6 and GST-PcfF.

relaxosome at the cell membrane independently of, but probably in spatial proximity to, PcfC. Upon generation of the PcfG–T-strand complex, one or both processing factors then deliver the transfer intermediate to the T4S receptor for translocation across the cell envelope.

Although several conjugative relaxases have been shown to interact directly with cognate substrate receptors in vitro (1, 65, 68), there also is increasing evidence that conjugative processing factors function as adaptors to spatially couple DNA substrate-T4S receptor binding reactions in vivo. For example, in the F plasmid transfer system, TraM stimulates TraI relaxase activity and also functions as a substrate specificity determinant by interacting with TraD via a C-terminal extension that is unique to this T4S receptor (8, 23, 49). Similarly, in the R388 plasmid transfer system, TrwA stimulates the nicking reaction through binding to *oriT* DNA and the TrwC relaxase (51, 52). TrwA interacts with the TrwB T4S receptor and also stimulates its ATPase activity, raising the intriguing possibility that substrate binding mediated through TrwA might activate TrwB and the cognate T4S system for translocation (65). In the *A. tumefaciens* VirB/D4 T4S system, the ParA/MinD homolog VirC1 and its interaction partner VirC2 stimulate VirD2-mediated cleavage at T-DNA border sequences, and VirC1 also recruits VirD2 and the T-DNA transfer intermediate to the polar-localized VirD4 receptor (2). Recently, cytosolic proteins termed VirD2 binding proteins also were shown to participate in polar recruitment of the relaxase, although the VirD2 binding proteins do not appear to be important for T-strand processing (34). Finally, MobB of plasmid R1162 functions together with the MobC accessory factor and MobA relaxase/primase to process IncQ plasmids. Reminiscent of PcfF, MobB stimulates MobA nicking at *oriT* and also might function as a spatial determinant for the relaxosome or the processed substrate, as suggested by recent evidence that MobB is an integral membrane protein, interacts with the MobA relaxase/primase, and mediates MobA translocation to recipient cells (55, 56).

Biochemical properties of PcfC. PcfC is most closely related to putative T4CPs associated with gram-positive conjugative plasmids and transposons, but it also resembles the well-characterized T4CPs of gram-negative systems (e.g., $VirD4_{At}$, $TraG_{RP4}$, and $TrwB_{R388}$) in molecular size, conservation of Walker A and B and other motifs, and overall secondary structure predicting an N-terminal membrane-spanning domain and a large cytosolic C-terminal domain (Fig. 1B) (60). Our in vitro studies of PcfCΔN103, the only gram-positive T4CP purified and characterized to date, identified biochemical properties similar to those reported for gram-negative T4CP's. As was the case for other T4CPs (60, 62, 65, 66), we were unable to purify sufficient amounts of soluble full-length PcfC for biochemical analysis, whereas the N-terminally truncated protein was readily purified. PcfCΔN103 fractionated exclusively as presumptive monomers by gel filtration (Fig. 5), also as shown for other N-terminally truncated T4CPs (39, 60). Interestingly, the soluble form of $TrwB_{R388}$ crystallized as a hexamer (29, 30), yet there also is evidence that $TrwB_{R388}$ and other T4CPs exist as monomeric and higher-order multimeric states in vivo, possibly in a dynamic equilibrium (60). Supporting this notion, $TrwB_{R388}$ recently was reported to form hexamers upon incubation with DNA or with the accessory processing factor TrwA (65). At this time, we have not detected similar shifts in PcfCΔN103 oligomerization in the presence of ss- or dsDNA substrates or the purified accessory factor PcfF (Y. Chen and H.-J. Yeo, unpublished data).

Purified forms of N-terminally truncated PcfC and the K156T mutant bound TNP-ATP with similar affinities, consistent with previous findings for $TrwB_{R388}$ and $TraG_{RP4}$ (39). Recently, truncated $TrwB_{R388}$ was shown to hydrolyze ATP in the presence of DNA oligonucleotides of a specific length and the processing factor TrwA (65, 66). An Ala substitution for Trp216 located in the internal channel of the TrwB hexamer abolished ATPase activity, although the ATPase activity of a K136T mutation corresponding to the PcfCK156T mutation was not characterized (66). Presently, we also have not detected PcfCΔN103 NTPase activity in the presence either of different DNA substrates or of purified accessory factor PcfF.

Our observations that the full-length PcfCK156T mutant displayed WT activities with respect to (i) membrane binding and spatial organization (Fig. 3), (ii) pCF10 substrate binding in vivo and nonspecific DNA binding in vitro (Fig. 4 and 5), and (iii) interactions with purified PcfF and PcfG in vitro (Y. Chen, unpublished findings) strongly indicate that the K156T mutation disrupts a stage of the transfer pathway subsequent to substrate processing and PcfC receptor docking. Similarly, in *A. tumefaciens*, VirD4Walker A mutants show no defects in spatial positioning or T-DNA substrate binding, and results of TrIP studies further indicate that VirD4 functions together with the VirB4 and VirB11 ATPases to energize T-DNA transfer across the inner membrane (3). pCF10 encodes a VirB4 ATPase homolog (PrgJ), a feature of all T4S systems characterized to date, and we recently determined that PcfC interacts with PrgJ in vitro (Y. Chen, unpublished data) consistent with a proposal that these two putative ATPases act together to energize translocation. The pCF10 transfer system lacks a VirB11 ATPase homolog, a feature also characteristic of most or all gram-positive bacterial T4S systems. Most gram-negative bacterial T4S systems possess VirB11 ATPases, although a few notable exceptions exist, such as the F plasmid conjugation system.

PcfCΔN103 bound nonspecifically and with similar affinities to dsDNA and ssDNA substrates (Fig. 5). The purified, N-terminally truncated T4CPs of the gram-negative systems similarly bind DNA without sequence specificity but vary in preferential binding to dsDNA (*Helicobacter pylori* HP0524) or ssDNA ($TrwB_{R388}$, $TraG_{RP4}$, and $TraD_F$) substrates (39, 50, 60, 62). In view of these nonspecific DNA binding properties, T4CPs most likely recognize cognate DNA substrates through a combination of interactions with the relaxase component of the transfer intermediate and other processing factors functioning as adaptors or spatial determinants. It is of interest that among the gram-negative conjugation systems, relaxases and other protein substrates carry C-terminal translocation signals comprised of clusters of positively charged residues that are necessary, albeit probably not sufficient, for substrate transfer (20, 40, 55, 67). PcfF and PcfG lack such C-terminal charge clusters, suggesting that other motifs confer substrate recognition in this gram-positive T4S system.

pCF10 T4S machine spatial organization. The spatial organization of bacterial secretion machines and other surface organelles has received considerable attention in recent years, but to date there are only a few reports describing the spatial distribution of T4S machines. Besides the polar-localized VirB/D4 T4S system of *A. tumefaciens* (4, 41, 44, 47), there is evidence that the Dot/Icm T4S machine assembles at the cell poles of *Legionella pneumophila* (J. Vogel, personal communication), whereas the plasmid R27 T4S system assembles at five or six places around the *E. coli* cell envelope (28). In gram-negative bacteria, the secretion channel and attachment organelle, e.g., the conjugative pilus, are generally considered to colocalize at the cell surface, with the latter playing a direct role in formation of productive mating pairs. By contrast, in the *E. faecalis* pCF10 system, we have shown that the AS surface adhesin and T4S system components assemble differently at cell the surface (Fig. 4). Thus, while AS functions to induce nonspecific cell clumping, it appears that only a subset of these cell-cell contacts progress to form mating junctions.

Factors governing the spatial distribution of AS and the T4S system components are unknown, but studies of other gram-positive secretion systems have identified potential localizing determinants, including membrane microdomains, cytoskeletal filaments, and components of the cell wall synthesis machinery (11, 13, 57). In *Streptococcus pyogenes*, for example, a single microdomain termed Exportal is enriched in anionic lipids and a high concentration of general secretory pathway translocons and represents the primary site for protein secretion across the cell envelope (58, 59).

By contrast, in rod-shaped *Bacillus subtilis* and *Listeria monocytogenes*, the general secretory pathway translocons are organized in spiral-like structures along the cell, also at sites enriched in anionic lipids (11, 13). Presently, we are exploring the basis for the spatial organization of the pCF10 T4S machine at the *E. faecalis* envelope, and we also are intrigued to investigate whether this apparatus dynamically redistributes as a function of cell growth, pheromone induction phase, or establishment of cell-cell contacts.

ACKNOWLEDGMENTS

We thank members of our laboratories for helpful comments and critiques of the manuscript. We thank W. Margolin for use of his fluorescence microscope facility and members of his laboratory for helpful comments.

This work was supported by NIH grants GM48746 (to P.J.C.) and GM49530 (to G.M.D.) and by Welch Foundation grant E-1616 (to H.-J.Y.).

REFERENCES

1. **Abajy, M. Y., J. Kopec, K. Schiwon, M. Burzynski, M. Doring, C. Bohn, and E. Grohmann.** 2007. A type IV-secretion-like system is required for conjugative DNA transport of broad-host-range plasmid pIP501 in gram-positive bacteria. J. Bacteriol. **189:**2487–2496.
2. **Atmakuri, K., E. Cascales, O. T. Burton, L. M. Banta, and P. J. Christie.** 2007. *Agrobacterium* ParA/MinD-like VirC1 spatially coordinates early conjugative DNA transfer reactions. EMBO J. **26:**2540–2551.
3. **Atmakuri, K., E. Cascales, and P. J. Christie.** 2004. Energetic components VirD4, VirB11 and VirB4 mediate early DNA transfer reactions required for bacterial type IV secretion. Mol. Microbiol. **54:**1199–1211.
4. **Atmakuri, K., Z. Ding, and P. J. Christie.** 2003. VirE2, a type IV secretion substrate, interacts with the VirD4 transfer protein at cell poles of *Agrobacterium tumefaciens*. Mol. Microbiol. **49:**1699–1713.
5. **Backert, S., and T. F. Meyer.** 2006. Type IV secretion systems and their effectors in bacterial pathogenesis. Curr. Opin. Microbiol. **9:**207–217.
6. **Baron, C.** 2005. From bioremediation to biowarfare: on the impact and mechanism of type IV secretion systems. FEMS Microbiol. Lett. **253:**163–170.
7. **Baron, C., and B. Coombes.** 2007. Targeting bacterial secretion systems: benefits of disarmament in the microcosm. Infect. Disord. Drug Targets **7:**19–27.
8. **Beranek, A., M. Zettl, K. Lorenzoni, A. Schauer, M. Manhart, and G. Koraimann.** 2004. Thirty-eight C-terminal amino acids of the coupling protein TraD of the F-like conjugative resistance plasmid R1 are required and sufficient to confer binding to the substrate selector protein TraM. J. Bacteriol. **186:**6999–7006.
9. **Berger, B. R., and P. J. Christie.** 1993. The *Agrobacterium tumefaciens virB4* gene product is an essential virulence protein requiring an intact nucleoside triphosphate-binding domain. J. Bacteriol. **175:**1723–1734.
10. **Bryan, E. M., T. Bae, M. Kleerebezem, and G. M. Dunny.** 2000. Improved vectors for nisin-controlled expression in gram-positive bacteria. Plasmid **44:**183–190.
11. **Buist, G., A. N. Ridder, J. Kok, and O. P. Kuipers.** 2006. Different subcellular locations of secretome components of Gram-positive bacteria. Microbiology **152:**2867–2874.
12. **Burgess, R. R., T. M. Arthur, and B. C. Pietz.** 2000. Mapping protein-protein interaction domains using ordered fragment ladder far-western analysis of hexahistidine-tagged fusion proteins. Methods Enzymol. **328:**141–157.
13. **Campo, N., H. Tjalsma, G. Buist, D. Stepniak, M. Meijer, M. Veenhuis, M. Westermann, J. P. Muller, S. Bron, J. Kok, O. P. Kuipers, and J. D. Jongbloed.** 2004. Subcellular sites for bacterial protein export. Mol. Microbiol. **53:**1583–1599.
14. **Caryl, J. A., M. C. Smith, and C. D. Thomas.** 2004. Reconstitution of a staphylococcal plasmid-protein relaxation complex in vitro. J. Bacteriol. **186:**3374–3383.
15. **Caryl, J. A., and C. D. Thomas.** 2006. Investigating the basis of substrate recognition in the pC221 relaxosome. Mol. Microbiol. **60:**1302–1318.
16. **Cascales, E., and P. J. Christie.** 2004. Definition of a bacterial type IV secretion pathway for a DNA substrate. Science **304:**1170–1173.
17. **Cascales, E., and P. J. Christie.** 2003. The versatile bacterial type IV secretion systems. Nat. Rev. Microbiol. **1:**137–150.
18. **Chen, Y., J. H. Staddon, and G. M. Dunny.** 2007. Specificity determinants of conjugative DNA processing in the *Enterococcus faecalis* plasmid pCF10 and the *Lactococcus lactis* plasmid pRS01. Mol. Microbiol. **63:**1549–1564.
19. **Christie, P. J.** 2004. Bacterial type IV secretion: the *Agrobacterium* VirB/D4 and related conjugation systems. Biochim. Biophys. Acta **1694:**219–234.
20. **Christie, P. J., K. Atmakuri, V. Krishnamoorthy, S. Jakubowski, and E. Cascales.** 2005. Biogenesis, architecture, and function of bacterial type IV secretion systems. Annu. Rev. Microbiol. **59:**451–485.
21. **Christie, P. J., and E. Cascales.** 2005. Structural and dynamic properties of bacterial type IV secretion systems. Mol. Membr. Biol. **22:**51–61.
22. **Christie, P. J., R. Z. Korman, S. A. Zahler, J. C. Adsit, and G. M. Dunny.** 1987. Two conjugation systems associated with *Streptococcus faecalis* plasmid pCF10: identification of a conjugative transposon that transfers between *S. faecalis* and *Bacillus subtilis*. J. Bacteriol. **169:**2529–2536.
23. **Disque-Kochem, C., and B. Dreiseikelmann.** 1997. The cytoplasmic DNA-binding protein TraM binds to the inner membrane protein TraD in vitro. J. Bacteriol. **179:**6133–6137.
24. **Dunny, G., C. Funk, and J. Adsit.** 1981. Direct stimulation of the transfer of antibiotic resistance by sex pheromones in *Streptococcus faecalis*. Plasmid **6:**270–278.
25. **Dunny, G. M.** 2007. The peptide pheromone-inducible conjugation system of *Enterococcus faecalis* plasmid pCF10: cell-cell signalling, gene transfer, complexity and evolution. Philos. Trans. R. Soc. London B **362:**1185–1193.
26. **Dunny, G. M., B. L. Brown, and D. B. Clewell.** 1978. Induced cell aggregation and mating in *Streptococcus faecalis*: evidence for a bacterial sex pheromone. Proc. Natl. Acad. Sci. USA **75:**3479–3483.
27. **Errington, J., J. Bath, and L. J. Wu.** 2001. DNA transport in bacteria. Nat. Rev. Mol. Cell Biol. **2:**538–545.
28. **Gilmour, M. W., T. D. Lawley, M. M. Rooker, P. J. Newnham, and D. E. Taylor.** 2001. Cellular location and temperature-dependent assembly of IncHI1 plasmid R27-encoded TrhC-associated conjugative transfer protein complexes. Mol. Microbiol. **42:**705–715.
29. **Gomis-Ruth, F. X., and M. Coll.** 2001. Structure of TrwB, a gatekeeper in bacterial conjugation. Int. J. Biochem. Cell Biol. **33:**839–843.
30. **Gomis-Ruth, F. X., M. Sola, F. de la Cruz, and M. Coll.** 2004. Coupling factors in macromolecular type-IV secretion machineries. Curr. Pharm. Des. **10:**1551–1565.
31. **Greve, B., S. Jensen, K. Brugger, W. Zillig, and R. A. Garrett.** 2004. Genomic comparison of archaeal conjugative plasmids from *Sulfolobus*. Archaea **1:**231–239.
32. **Grohmann, E., G. Muth, and M. Espinosa.** 2003. Conjugative plasmid transfer in gram-positive bacteria. Microbiol. Mol. Biol. Rev. **67:**277–2301.
33. **Guasch, A., M. Lucas, G. Moncalian, M. Cabezas, R. Perez-Luque, F. X. Gomis-Ruth, F. de la Cruz, and M. Coll.** 2003. Recognition and processing of the origin of transfer DNA by conjugative relaxase TrwC. Nat. Struct. Biol. **10:**1002–1010.
34. **Guo, M., S. Jin, D. Sun, C. L. Hew, and S. Q. Pan.** 2007. Recruitment of conjugative DNA transfer substrate to *Agrobacterium* type IV secretion apparatus. Proc. Natl. Acad. Sci. USA **104:**20019–20024.
35. **Hayes, F., C. Daly, and G. F. Fitzgerald.** 1990. Identification of the minimal replicon of *Lactococcus lactis* subsp. *lactis* UC317 plasmid pCI305. Appl. Environ. Microbiol. **56:**202–209.
36. **Hiratsuka, T., and K. Uchida.** 1973. Preparation and properties of 2′(or 3′)-O-(2,4,6-trinitrophenyl) adenosine 5′-triphosphate, an analog of adenosine triphosphate. Biochim. Biophys. Acta **320:**635–647.
37. **Hirt, H., S. L. Erlandsen, and G. M. Dunny.** 2000. Heterologous inducible expression of *Enterococcus faecalis* pCF10 aggregation substance asc10 in *Lactococcus lactis* and *Streptococcus gordonii* contributes to cell hydrophobicity and adhesion to fibrin. J. Bacteriol. **182:**2299–2306.
38. **Hirt, H., D. A. Manias, E. M. Bryan, J. R. Klein, J. K. Marklund, J. H. Staddon, M. L. Paustian, V. Kapur, and G. M. Dunny.** 2005. Characterization of the pheromone response of the *Enterococcus faecalis* conjugative plasmid pCF10: complete sequence and comparative analysis of the transcriptional and phenotypic responses of pCF10-containing cells to pheromone induction. J. Bacteriol. **187:**1044–1054.
39. **Hormaeche, I., I. Alkorta, F. Moro, J. M. Valpuesta, F. M. Goni, and F. De La Cruz.** 2002. Purification and properties of TrwB, a hexameric, ATP-binding integral membrane protein essential for R388 plasmid conjugation. J. Biol. Chem. **277:**46456–46462.
40. **Jakubowski, S. J., E. Cascales, V. Krishnamoorthy, and P. J. Christie.** 2005. *Agrobacterium tumefaciens* VirB9, an outer-membrane-associated component of a type IV secretion system, regulates substrate selection and T-pilus biogenesis. J. Bacteriol. **187:**3486–3495.
41. **Judd, P. K., R. B. Kumar, and A. Das.** 2005. Spatial location and requirements for the assembly of the *Agrobacterium tumefaciens* type IV secretion apparatus. Proc. Natl. Acad. Sci. USA **102:**11498–11503.
42. **Kristich, C. J., J. R. Chandler, and G. M. Dunny.** 2007. Development of a host-genotype-independent counterselectable marker and a high-frequency conjugative delivery system and their use in genetic analysis of *Enterococcus faecalis*. Plasmid **57:**131–144.
43. **Kristich, C. J., D. A. Manias, and G. M. Dunny.** 2005. Development of a method for markerless genetic exchange in *Enterococcus faecalis* and its use in construction of a *srtA* mutant. Appl. Environ. Microbiol. **71:**5837–5849.
44. **Kumar, R. B., and A. Das.** 2002. Polar location and functional domains of the *Agrobacterium tumefaciens* DNA transfer protein VirD4. Mol. Microbiol. **43:**1523–1532.
45. **Kuo, M. H., and C. D. Allis.** 1999. *In vivo* cross-linking and immunoprecipitation for studying dynamic protein:DNA associations in a chromatin environment. Methods **19:**425–433.
46. **Kurenbach, B., J. Kopec, M. Magdefrau, K. Andreas, W. Keller, C. Bohn, M. Y. Abajy, and E. Grohmann.** 2006. The TraA relaxase autoregulates the putative type IV secretion-like system encoded by the broad-host-range *Streptococcus agalactiae* plasmid pIP501. Microbiology **152:**637–645.
47. **Lai, E. M., O. Chesnokova, L. M. Banta, and C. I. Kado.** 2000. Genetic and environmental factors affecting T-pilin export and T-pilus biogenesis in relation to flagellation of *Agrobacterium tumefaciens*. J. Bacteriol. **182:**3705–3716.
48. **Leenhouts, K., G. Buist, A. Bolhuis, A. ten Berge, J. Kiel, I. Mierau, M. Dabrowska, G. Venema, and J. Kok.** 1996. A general system for generating

unlabelled gene replacements in bacterial chromosomes. Mol. Gen. Genet. **253:**217–224.
49. **Lu, J., and L. S. Frost.** 2005. Mutations in the C-terminal region of TraM provide evidence for in vivo TraM-TraD interactions during F-plasmid conjugation. J. Bacteriol. **187:**4767–4773.
50. **Moncalian, G., E. Cabezon, I. Alkorta, M. Valle, F. Moro, J. M. Valpuesta, F. M. Goni, and F. de La Cruz.** 1999. Characterization of ATP and DNA binding activities of TrwB, the coupling protein essential in plasmid R388 conjugation. J. Biol. Chem. **274:**36117–36124.
51. **Moncalian, G., and F. de la Cruz.** 2004. DNA binding properties of protein TrwA, a possible structural variant of the Arc repressor superfamily. Biochim. Biophys. Acta **1701:**15–23.
52. **Moncalian, G., G. Grandoso, M. Llosa, and F. de la Cruz.** 1997. *oriT*-processing and regulatory roles of TrwA protein in plasmid R388 conjugation. J. Mol. Biol. **270:**188–200.
53. **Ninio, S., and C. R. Roy.** 2007. Effector proteins translocated by *Legionella pneumophila*: strength in numbers. Trends Microbiol. **15:**372–380.
54. **Olmsted, S. B., S. L. Erlandsen, G. M. Dunny, and C. L. Wells.** 1993. High-resolution visualization by field emission scanning electron microscopy of *Enterococcus faecalis* surface proteins encoded by the pheromone-inducible conjugative plasmid pCF10. J. Bacteriol. **175:**6229–6237.
55. **Parker, C., and R. J. Meyer.** 2007. The R1162 relaxase/primase contains two, type IV transport signals that require the small plasmid protein MobB. Mol. Microbiol. **66:**252–261.
56. **Perwez, T., and R. Meyer.** 1996. MobB protein stimulates nicking at the R1162 origin of transfer by increasing the proportion of complexed plasmid DNA. J. Bacteriol. **178:**5762–5767.
57. **Pugsley, A. P., and N. Buddelmeijer.** 2004. Traffic spotting: poles apart. Mol. Microbiol. **53:**1559–1562.
58. **Rosch, J., and M. Caparon.** 2004. A microdomain for protein secretion in Gram-positive bacteria. Science **304:**1513–1515.
59. **Rosch, J. W., and M. G. Caparon.** 2005. The ExPortal: an organelle dedicated to the biogenesis of secreted proteins in *Streptococcus pyogenes*. Mol. Microbiol. **58:**959–968.
60. **Schroder, G., S. Krause, E. L. Zechner, B. Traxler, H. J. Yeo, R. Lurz, G. Waksman, and E. Lanka.** 2002. TraG-like proteins of DNA transfer systems and of the *Helicobacter pylori* type IV secretion system: inner membrane gate for exported substrates? J. Bacteriol. **184:**2767–2779.
61. **Schroder, G., and E. Lanka.** 2005. The mating pair formation system of conjugative plasmids—a versatile secretion machinery for transfer of proteins and DNA. Plasmid **54:**1–25.
62. **Schroder, G., and E. Lanka.** 2003. TraG-like proteins of type IV secretion systems: functional dissection of the multiple activities of TraG (RP4) and TrwB (R388). J. Bacteriol. **185:**4371–4381.
63. **Smith, M. C., and C. D. Thomas.** 2004. An accessory protein is required for relaxosome formation by small staphylococcal plasmids. J. Bacteriol. **186:** 3363–3373.
64. **Staddon, J. H., E. M. Bryan, D. A. Manias, Y. Chen, and G. M. Dunny.** 2006. Genetic characterization of the conjugative DNA processing system of enterococcal plasmid pCF10. Plasmid **56:**102–111.
65. **Tato, I., I. Matilla, I. Arechaga, S. Zunzunegui, F. de la Cruz, and E. Cabezon.** 2007. The ATPase activity of the DNA transporter TrwB is modulated by protein TrwA: implications for a common assembly mechanism of DNA translocating motors. J. Biol. Chem. **282:**25569–25576.
66. **Tato, I., S. Zunzunegui, F. de la Cruz, and E. Cabezon.** 2005. TrwB, the coupling protein involved in DNA transport during bacterial conjugation, is a DNA dependent ATPase. Proc. Natl. Acad. Sci. USA **102:**8156–8161.
67. **Vergunst, A. C., M. C. van Lier, A. den Dulk-Ras, T. A. Grosse Stuve, A. Ouwehand, and P. J. Hooykaas.** 2005. Positive charge is an important feature of the C-terminal transport signal of the VirB/D4-translocated proteins of *Agrobacterium*. Proc. Natl. Acad. Sci. USA **102:**832–837.
68. **Waters, C. M., and G. M. Dunny.** 2001. Analysis of functional domains of the *Enterococcus faecalis* pheromone-induced surface protein aggregation substance. J. Bacteriol. **183:**5659–5667.
69. **Waters, C. M., C. L. Wells, and G. M. Dunny.** 2003. The aggregation domain of aggregation substance, not the RGD motifs, is critical for efficient internalization by HT-29 enterocytes. Infect. Immun. **71:**5682–5689.
70. **Zhou, L., D. A. Manias, and G. M. Dunny.** 2000. Regulation of intron function: efficient splicing *in vivo* of a bacterial group II intron requires a functional promoter within the intron. Mol. Microbiol. **37:**639–651.